ISSN (Print) 1226-1750
ISSN (Online) 2233-6656
Journal of Magnetics 26(1), 79-86 (2021) https://doi.org/10.4283/JMAG.2021.26.1.079

Magnetic Field Model of Macro-motion of Coaxial Integrated Macro-micro Composite Actuator

Caofeng Yu*, Zhuo Chen, Meijun Xiong, Yu Wang, Rui Shi, and Xiaoxiang Sun

School of Mechanical Engineering, Anhui University of Science and Technology, Huainan 232001, Anhui, China

(Received 24 September 2020, Received in final form 23 January 2021, Accepted 25 January 2021)

Aiming at the problem of short stroke of giant magnetostrictive actuator (GMA), a design scheme of coaxial integrated macro-micro composite actuator is proposed by combining the long-stroke characteristics of voice coil motor with the high-precision characteristics of giant magnetostrictive actuator. Based on its structure composition and working principle, the magnetic field model of macro-motion of macro-micro composite actuator is established based on the analysis method of circuit, and the change characteristics of the driving magnetic field are obtained. The finite element method is used to verify the magnetic circuit characteristics. The results show that the magnetic circuit variation characteristics of the proposed coaxial integrated macro-micro composite actuator are consistent with the theoretical calculation results, and are consistent with the expected working process of this actuator, which indicates that the established magnetic field model is correct, and that the proposed coaxial integrated design scheme of the macro-micro composite actuator is feasible.

Keywords : magnetic field model, giant magnetostrictive actuator, voice coil motor, coaxial integrated, actuator

1. Introduction

Precision manufacturing industry is the strong driving force for the development of national manufacturing industry. With the rapid development of precision manufacturing industry, the requirement of miniaturization, precision and mass production for precision parts is put forward, which makes the performance requirement of precision manufacturing equipment for precision parts processing continuously improve. The research and development of precision manufacturing equipment with comprehensive characteristics of high speed, high acceleration, high precision and long stroke has become one of the important research subjects [1, 2].

Driving system is the key core component of precision manufacturing equipment, and its performance directly affects the performance of precision manufacturing equipment [3, 4]. At present, the research focus of scholars at home and abroad is on the macro and micro power sources, that is to select different combination of power sources to increase the positioning stroke and improve the positioning accuracy. For example, McMaster University of Canada [5] has developed a large stroke two-dimensional macro micro dual drive system. The experimental results show that the tracking error of dual drive positioning is reduced by about 83 % compared with that of single linear motor drive. The integrated solution company [6] of the United States has developed a precision positioning table for lithography and the positioning accuracy of the system can reach 20 nm. Tokyo University of Japan [7] has designed a macro micro drive device. The experiment shows that the macro motion accuracy of the whole driving device is 5 μm and the micro motion accuracy is 20 nm. Pahk *et al.* [8] of Seoul University of Korea designed a macro-micro drive device, which uses traditional servo motor to drive ball screw to realize macro motion, piezoelectric ceramics to realize micro motion, so as to realize the positioning accuracy of 10 nm. Professor Zhu of Tsinghua University [9] cooperated with Shanghai Microelectronics Equipment Co., Ltd. to develop a lithography machine motion platform which uses linear motor to drive macro stage, air bearing and voice coil motor to drive micro stage, with a working stroke of 300 mm and a positioning accuracy of 12 nm. Professor Wang of Harbin University of Technology [10] has successfully developed an ultra-precision positioning workbench with a working stroke of 500 mm and a repetitive positioning accuracy of 20 nm. Professor Zhang

*Corresponding author: Tel: +86-13645547192
Fax: +86+0054-6668917, e-mail: yucaofeng@aust.edu.cn

of South China Agricultural University [11] designed a macro-micro drive cylindrical linear piezoelectric motor. Compared with piezoelectric ceramics, the axial deformation of the micro structure increases by about 8.45 times. In addition, Professor Bai [12], Professor Chen [13], Professor Long [14], Professor Duan [15], Professor Zhang [16] and Dr. Teng [17] designed different macro and micro composite platforms with different control methods, and achieved good control results.

In conclusion, There are two main forms of macro-micro composite actuator structure, one is stack superposition and the other is coaxial alignment. The stack superposition is to superimpose the micro actuator over the macro actuator and drive the micro actuator to move together when the macro actuator moves. This installation method is simple and easy to implement, but the macro/micro actuator is not on the same axis. The Abbe error will occur when measuring displacement, which results in inaccurate displacement measurement and affects control accuracy. The coaxial alignment is to move the macro actuator and the micro actuator. The two actuators are placed at both ends of the workbench and aligned with their axes. Although this installation method can avoid Abbe error when measuring displacement, it is necessary to keep the axis alignment of macro/micro actuator when installing, which imposes high requirements on the structure installation and the overall structure of the workbench is complicated. Therefore, in order to overcome the shortcomings of existing macro-micro composite actuator mode, based on the electromagnetic drive principle of voice coil motor and magnetostriction effect of giant magnetostrictive material, this paper proposes a coaxial integration scheme of macro-micro composite actuator with simple structure, easy installation and no Abbe error. Based on the analysis method of "circuit", the magnetic field model of macro-micro composite actuator is established and the change characteristics of the driving magnetic field are obtained. The characteristics of magnetic circuit are verified by finite element simulation analysis. Finally, a coaxial integration design scheme of macro-micro composite actuator is determined, which can solve the Abbe error problem of existing macro-micro composite actuator structure and lay a theoretical foundation for high-performance actuator in precision manufacturing field.

2. Structure and Working Principle of Coaxial Integrated Macro-micro

2.1. Structure of coaxial integrated macro-micro composite actuator

The structure of coaxial integrated macro-micro composite actuator proposed in this work is shown in Fig. 1. It consists of shell, tile permanent magnet, macro-coil, macro-coil skeleton, micro-coil, micro-coil skeleton, disc spring, output rod, end cover, etc. The inner wall of the shell is fixed with annular permanent magnet, and the macro-coil framework is placed inside the annular permanent magnet body, and the macro-coil framework is outside the annular permanent magnet body. The micro-coil skeleton is set inside the macro coil skeleton, the micro coil skeleton is connected outside the micro coil skeleton, the giant magnetostrictive material (GMM) rod is placed inside the micro-coil skeleton, and both ends of the GMR are provided with magnetic conducting blocks to increase the magnetic field intensity of the axis position; the cooling pipe is connected around the GMM rod periphery. It is used for heat dissipation to ensure the performance of GMR.

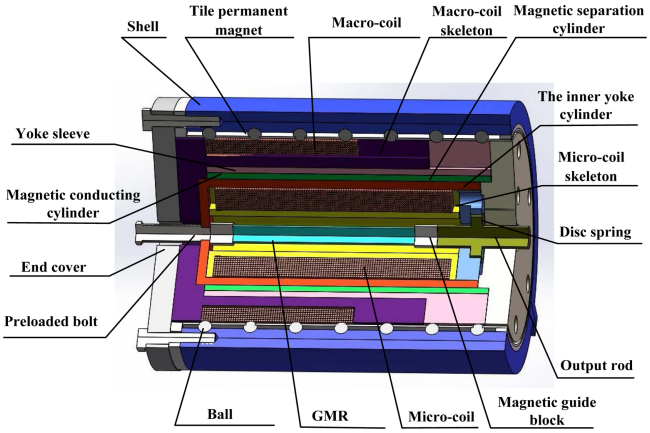

Fig. 1. (Color online) Three dimensional cross section diagram of coaxial integrated macro-micro composite actuator.

2.2. Working principle of coaxial integrated macro-micro composite actuator

The working process of the coaxial integrated macro-micro composite actuator proposed in this work is divided into three stages: the initial zero stage, the macro positioning stage and the micro compensation stage. The working principle of each stage of macro-micro composite actuator is as follows and the motion process of macro-micro composite actuator is as show in Fig. 2.

(1) Initial zero-position stage: at this stage, the macro-micro composite actuatorr is in zero-position, i.e. the inner coil of the driver is not connected to the power supply, and both the macro and micro components are in zero-position.

(2) Macro positioning stage: the tiled permanent magnet generates a constant magnetic field B inside the magnet along the radial direction of the driver; the length of the

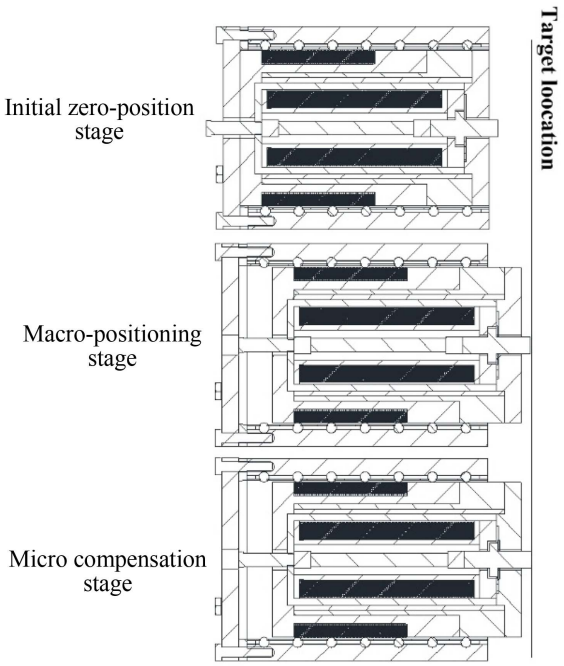

Fig. 2. Schematic diagram of three motion states of coaxial integrated macro-micro composite actuator.

macro coil is set to L. When the macro coil passes through the current I_{ma}, according to the Ampere law, the macro coil will be affected by Ampere Force F at this time. The value is $BI_{ma}L$, according to the left-hand rule, can determine the direction of force along the axis of the driver; under the action of Ampere force F, the macro coil and the macro coil frame together with all its internal components move along the axis of the driver, thus realizing the macro positioning process; by adjusting the I_{ma} value of the current of the macro coil, the magnitude of force F can be controlled. As the frame of the macro coil is made of ferrous material, it will be blocked from moving outwards by the electromagnetic force F_1 of the tiled permanent magnet, and F_1 will increase with the distance of the macro coil frame moving outwards. When F_1=F is equal, the macro motion will reach balance. Therefore, the acceleration, speed and distance of the macro moving parts can be controlled by adjusting the I_{ma} value.

(3) Micro compensation stage: the function of micro stage is to compensate the macro positioning process. Its working principle is that when there is deviation Δx between the macro positioning distance and the ideal positioning distance, current I_{mi} is applied to the micro coil, which forms an electrified solenoid and generates magnetic field H along the axis in the micro coil. Because the GMM rod has magnetostriction effect, the magnetic field strength H is increased at the magnetic field strength H. Under the action of this function, the GMM rod will deform and extend, push the output rod to compress the disc spring, so that the output rod will generate output displacement and realize micro-movement. By adjusting the current I_{mi} value of the micro-coil, the size of the generated magnetic field H can be controlled, and then the extension of the GMM rod can be adjusted, the micro-displacement value can be controlled close to Δx, and the macro positioning error can be compensated to improve the overall positioning accuracy of the actuator. Ultra-precise positioning of macro-micro composite actuators over a large stroke range can be achieved by comprehensively adjusting the I_{ma} value of macro-coil current and the I_{mi} value of micro-coil current.

3. Magnetic Field Model of Coaxial Integrated Macro-micro Composite Actuator for Macro-motion

According to the structure design scheme of the coaxial integrated macro-micro composite actuator, the magnetic flux distribution structure diagram of the macro and micro composite actuator is obtained and as shown in Fig. 3, which contains two magnetic field sources, namely permanent magnet and energized coil. When a constant current I is applied to the coil, the magnetic field generated by the coil will be superimposed with the magnetic field generated by the permanent magnet. Based on the "circuit" analysis method, it can be equivalent to the circuit with multiple voltage sources. The flux loops with magnetic potential distribution are named S_1 and S_2 respectively, and the counterclockwise direction is positive.

Two equal magnetomotive forces are generated by macro-motion coil, which are expressed by F_{n1} and F_{n2} respectively, and their values can be expressed by formula (1) where N_1 represents the turns of macro-motion coil,

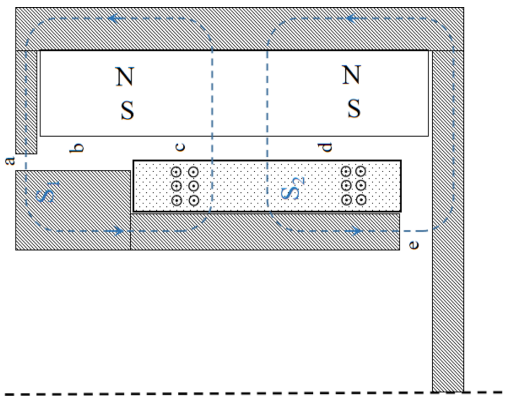

Fig. 3. (Color online) Schematic diagram of magnetic flux distribution of macro-motion magnetic field of coaxial integrated macro-micro composite actuator.

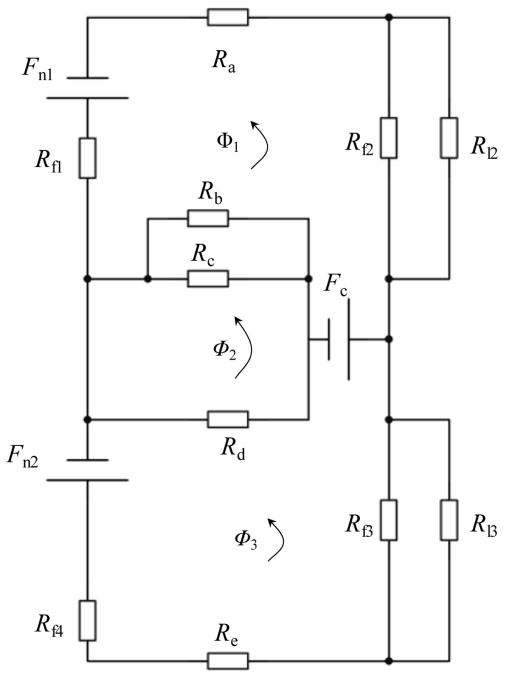

Fig. 4. Equivalent magnetic circuit model of magnetic field for macro-motion of coaxial integrated macro-micro composite actuator.

and I_1 means the current of macro-motion coil. Let R_c be the magnetoresistance of air gap b and c in parallel, R_{f1}, R_{f2}, R_{f3} and R_{f4} as the magnetic resistance of soft magnetic conductive materials, R_{l2} and R_{l3} as leakage reluctance, R_a, R_b, R_c, R_d, R_e as air gap magnetoresistance, Φ_1, Φ_2, Φ_3 as the magnetic flux of each loop, H_c as the coercivity of permanent magnet and h has the radial thickness of permanent magnet, F_c as the magnetomotive force of tile permanent magnet. According to the basic magnetic circuit law and the circuit analysis method with multiple sources, the equivalent magnetic circuit model of the coaxial integrated macro-micro composite actuator is obtained, as shown in Fig. 4.

The magnetic field model of the coaxial integrated macro-micro composite actuator for macro-motion is obtained by combining the mesh current method of the circuit as follows (1):

$$\begin{cases} F_{n1}+F_c=(R_a+\dfrac{1}{\dfrac{1}{R_{f2}}+\dfrac{1}{R_{l2}}}+R_{f1}+R_c)\cdot\Phi_1-R_c\cdot\Phi_2 \\ F_{n2}-F_c=(R_e+R_{f4}+\dfrac{1}{\dfrac{1}{R_{f3}}+\dfrac{1}{R_{l3}}}+R_d)\cdot\Phi_3-R_d\cdot\Phi_2 \\ -R_d\cdot\Phi_3-R_c\cdot\Phi_1+(R_d+R_c)\Phi_2=F_{n2} \\ F_{n1}=F_{n2}=N_1I_1 \\ F_c=H_ch \end{cases} \tag{1}$$

Because the relative magnetic permeability of the soft iron material μ_r is much larger than that of the air μ_0. That is, the core magnetoresistance of the soft iron material in the coaxial integrated macro-micro composite actuator is much smaller than that of the air gap magnetoresistance. Therefore, for the convenience of magnetic field analysis, the following assumptions are made:

a) The magnetic circuit returns to the magnetic pole through the air gap and permanent magnet, where the magnetic induction intensity is uniform and perpendicular to the outer yoke barrel and coil.

b) Coil winding and soft magnetic material are ideal uniform materials, and the magnetic leakage resistance and the magnetic resistance of soft magnetic material can be neglected.

c) Permanent magnet and air gap permeability are equal.

Based on the above assumptions, Formula (1) can be simplified to:

$$\begin{cases} N_1I_1+H_ch=(R_a+R_c)\Phi_1-R_c\Phi_2 \\ N_1I_1-H_ch=(R_e+R_d)\Phi_3-R_d\Phi_2 \\ -R_d\Phi_3-R_c\Phi_1+(R_c+R_d)\Phi_2=0 \end{cases} \tag{2}$$

The equation group (2) is solved and simplified to obtain:

$$\begin{cases} \Phi_1=\dfrac{(2R_cR_d+R_c\,R_e+R_dR_e)N_1I_1+(R_cR_e+R_dR_e)H_ch}{R_aR_cR_d+R_aR_c\,R_e+R_aR_dR_e+R_cR_dR_e} \\ \Phi_2=\dfrac{(R_aR_d+R_c\,R_e-2R_cR_d)N_1I_1+(R_cR_e+R_aR_d)H_ch}{R_aR_cR_d+R_aR_c\,R_e+R_aR_dR_e+R_cR_dR_e} \\ \Phi_3=\dfrac{(R_aR_c+R_a\,R_d+2R_cR_d)N_1I_1-(R_aR_c+R_aR_d)H_ch}{R_aR_cR_d+R_aR_c\,R_e+R_aR_dR_e+R_cR_dR_e} \end{cases} \tag{3}$$

The magnetic induction B_i at the air gap is related to the area S_i through which the magnetic flux passes:

$$B_i=\frac{\Phi_i}{S_i} \tag{4}$$

According to equation (4), the magnetic induction intensity of air gap at a, b, c, d and e is calculated as follows:

$$\begin{cases} B_a=\dfrac{\Phi_1}{S_a} \\ B_b=\dfrac{R_c\Phi_1}{S_b(R_c+R_b)} \\ B_c=\dfrac{\dfrac{R_b}{R_c+R_b}\Phi_1-R_c\Phi_2}{S_c} \\ B_d=\dfrac{\Phi_2-\Phi_3}{S_d} \\ B_e=\dfrac{\Phi_3}{S_d} \end{cases} \tag{5}$$

Table 1. Structural parameters for coaxial integrated macro-micro composite actuator at initial position.

Parameters	External radius R/mm	Inner radius r/mm	Inner radius r/mm	Average Flux Area/m^2
Air gap a	50	45	5	0.00149
Air gap b	50	45	40	0.0119
Air gap c	50	38	38	0.0105
Air gap d	50	38	38	0.0105
Parameter	Floor area/m^2		Bottom area/m^2	Initial air gap length/m
Air gap e	0.00128		0.00408	0.012

The calculation formula of air gap reluctance is:

$$R_i = \frac{g_i}{Su_0} \tag{6}$$

Where g_i is the length of air gap i and S is the interpole area.

Table 1 shows the structural design parameters of coaxial integrated macro-micro composite actuator at initial position. According to the air gap reluctance calculation formula, the air gap reluctance values of R_a, R_b, R_c, R_d and R_e at initial position are calculated as shown in Table 2.

By substituting the calculated reluctance value into the air gap flux expression (3) and the air gap magnetic induction intensity calculation (5), the following results are obtained:

$$\begin{cases} \Phi_1 > 0 \\ \Phi_2 > 0 \\ \Phi_3 < 0 \\ |\Phi_1| > |\Phi_3| \\ B_a > B_d > B_e > B_b > B_c \end{cases} \tag{7}$$

When the coaxial integrated macro-micro composite actuator operates, the outer yoke barrel will move outwards, increasing the air gap at e and thus the reluctance R_e at e. According to the expressions of Φ_1 and B_a, the curves of Φ_1 and B_a with movement displacement are obtained as shown in Fig. 5.

It can be seen from Fig. 5 that both Φ_1 and B_a decrease with the increase of displacement, that is, with the increase of magnetoresistance R_e.

Table 2. Calculated values of magnetic resistance in each air gap of macro-micro composite actuator.

Parameters	Numerical values (1/H)
Air gap reluctance R_a	2.6×10^6
Air gap reluctance R_b	0.332×10^6
Air gap reluctance R_c	0.913×10^6
Air gap reluctance R_d	0.913×10^6
Air gap reluctance R_e	7.5×10^6

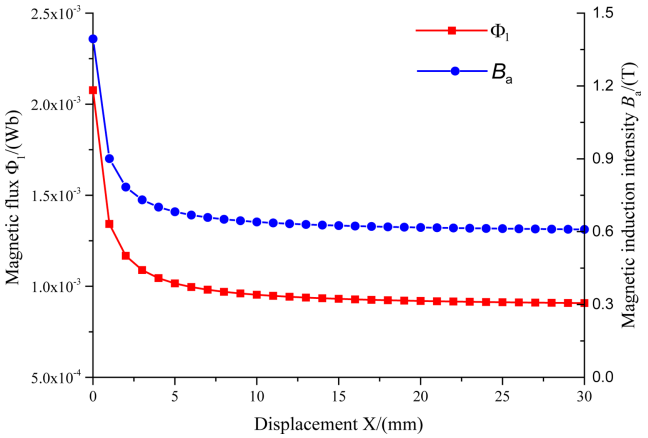

Fig. 5. (Color online) Variation curve of magnetic flux Φ_1 and magnetic induction B_a of coaxial integrated macro-micro composite actuator.

Similarly, with the increase of displacement, R_e increases, the average flux density of air gap at c increases, and the average flux density of air gap at d decreases.

The Thevenin equivalent circuit method shows that a two-terminal network consisting of multiple sources and resistors can be equivalent to a voltage source and a resistor in series. Therefore, the equivalent circuit of the

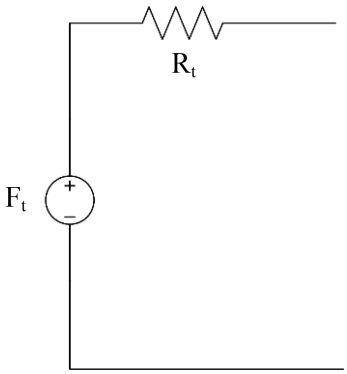

Fig. 6. Schematic diagram of Thevenin equivalent magnetic circuit model of coaxial integrated macro-micro composite actuator.

magnetic circuit of the macro-micro composite actuator can be obtained as shown in Fig. 6.

In Fig. 6, F_t is the equivalent magneto-dynamic potential of the reluctance circuit and R_t is the equivalent total reluctance. Close both ends of the equivalent magnetic circuit:

$$\Phi = \frac{F_t}{R_t} \tag{8}$$

In equation (8), Φ is the total flux. During the macro motion of the actuator, the equivalent magnetomotive force F_t remains unchanged, while the equivalent total magnetoresistance R_t increases, so the total magnetic flux Φ decreases.

4. Simulation Analysis and Model Topology of Magnetic Field Model

In order to verify the correctness of the established macro drive magnetic field model and prediction results, COMSOL Multiphysics software is used to carry out finite element simulation analysis of electromagnetic field.

It can be seen from the structure of coaxial integrated macro-micro composite actuator that its magnetic circuit is 3D axisymmetric structure. In order to improve the accuracy and efficiency of the model analysis, the finite element model of the driver is established by two-dimensional axisymmetric analysis in AC/DC (electromagnetic field) module of COMSOL software, and the macro part is appropriately simplified. The simplified model shown in Fig. 7 (right) is obtained, in which the relevant parameters of simulation are shown in Table 3.

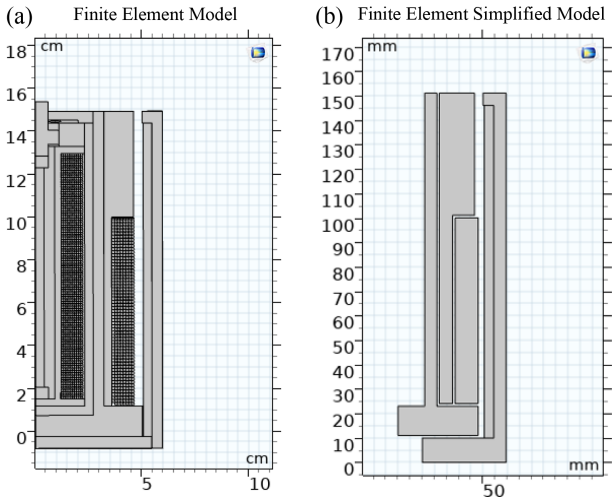

Fig. 7. (Color online) The established two dimensional finite element model of macro-micro composite actuator. (a) Before simplification, (b) After simplification.

Table 3. Related parameters of magnetic field simulation of macro-micro composite actuator.

Parameters	Values
NdFeB ($Nd_{0.7}FeB$) Residual flux density B_r	1.20T~1.24T
NdFeB ($Nd_{0.7}FePB$) Coercivity H_c	830~880 KA/m
NdFeB ($Nd_{0.7}FeB$) Maximum magnetic energy product BH	310 KJ/m^3
Cross sectional area of conductor	1 mm^2
Wire turns N	400
Current is applied to the wire I	6A
Relative permeability of soft iron μ	4000
Mesh size	Very fine (0.007 mm~3.5 mm)
Macro displacement	0 mm~30 mm

The electromagnetic field distribution at the macro displacement of 0 mm, 10 mm and 30 mm is calculated respectively. The magnetic field distribution cloud diagram and magnetic line distribution are shown in Fig. 8.

From Fig. 8, it can be seen that the flux density distribution in S_1 circuit is larger than that in S_2 circuit, and the flow direction of S_1 and S_2 magnetic field is opposite; the magnetic lines are distributed in reverse and upward directions, and the magnetic lines at the upper end of section are denser than those at the lower end. The calculated results based on the established drive magnetic field model are $\Phi_1 > 0$, $\Phi_2 > 0$, $\Phi_3 < 0$ and $|\Phi_1| > |\Phi_3|$. Among them, Φ_1 is the magnetic flux loop value of S_1 circuit, and its value is greater than 0; Φ_3 is the magnetic flux loop value of S_2, and its value is less than 0. This is in agreement with the simulation results.

In electromagnetic field simulation, the average magnetic flux density of each air gap is recorded with each 10 mm movement of the macro yoke. The expression of the average magnetic flux density of each air gap is:

$$\overline{B}_i = \frac{B_{i\max} + B_{i\min}}{2} \tag{9}$$

In equation (9), $B_{i\max}$ is the maximum flux density at the air gap and $B_{i\min}$ is the minimum flux density at the air gap. The average magnetic flux density values at a, b, c, d and e are recorded as shown in Table 4. The maximum magnetic flux density mode in the driver interface during macro-operation is shown in Fig. 9.

It can be seen from Fig. 9 that with the increase of macrodynamic displacement, the average magnetic flux density of air gap at a, d and e decreases, while the average magnetic flux density of air gap at b and c increases. This is in agreement with the calculation results of the

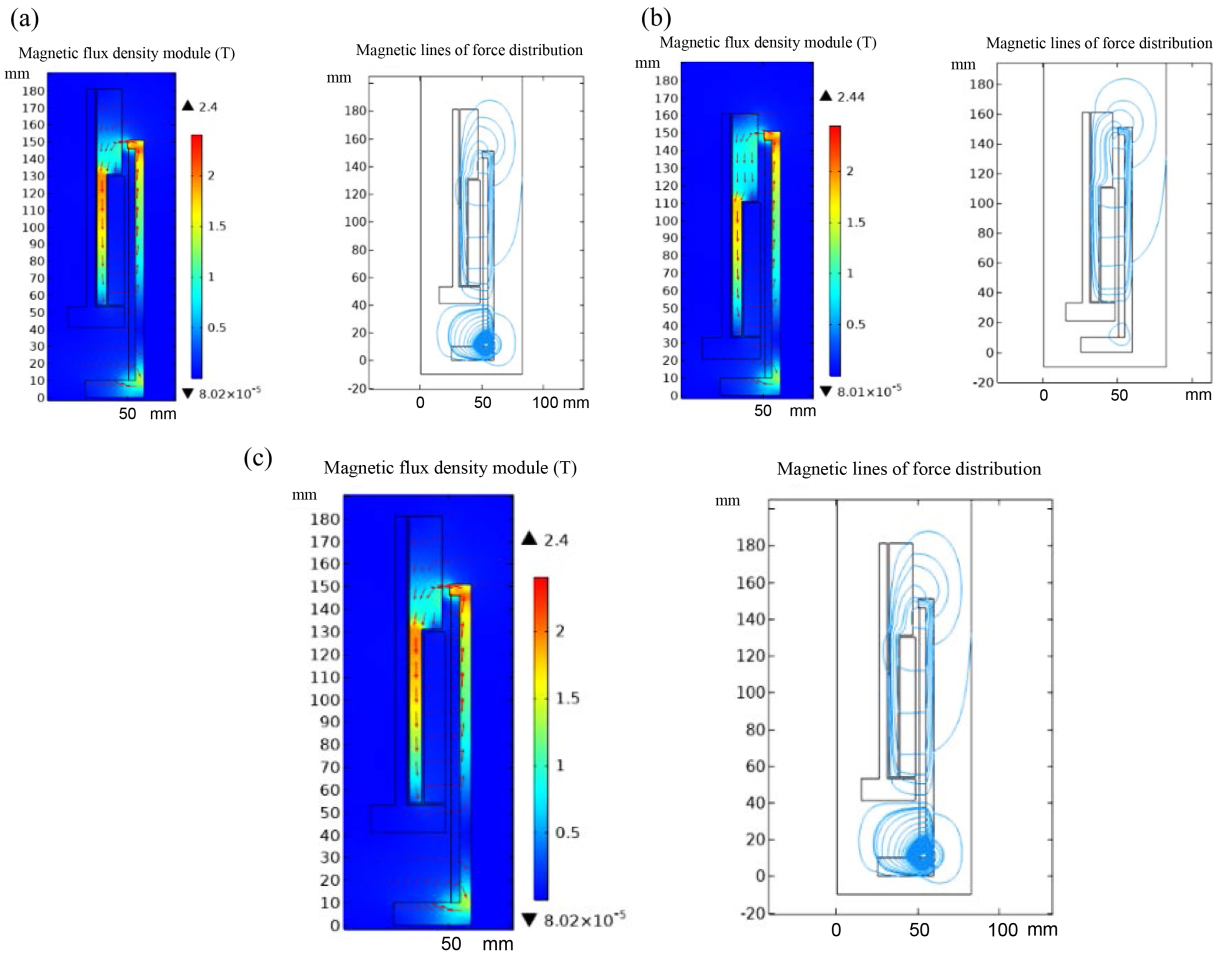

Fig. 8. Distribution of magnetic flux density and magnetic line of force in the cross section of macro-micro composite actuator with different macro-motion displacements. (a) The macro-motion coil displacement is 0 mm (b) The macro-motion displacement is 10 mm (c) The macro-motion coil displacement is 30 mm.

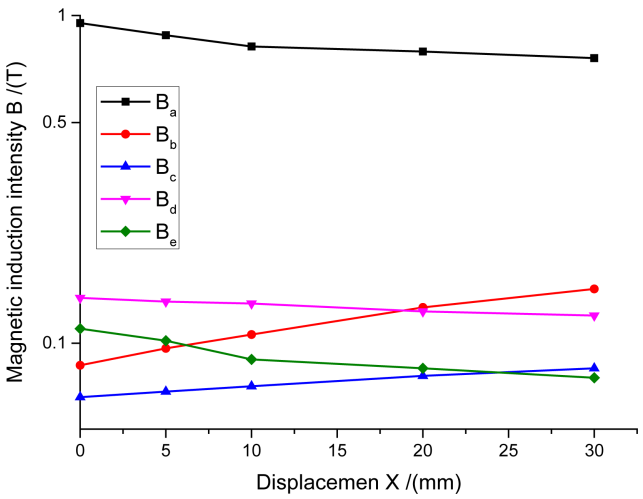

Fig. 9. (Color online) Variation trend of average flux density in air gap under different macro-motion displacements of macro-micro composite actuator.

magnetic field model established in this paper. At the same time, with the movement of the macro-actuator, the total flux density in the cross-section of the macro-micro composite actuator decreases while the magnetic potential of the permanent magnet remains unchanged and the excitation of the coil remains unchanged. This is also consistent with the calculation results of the drive magnetic field model established in this paper.

5. Conclusion

In this paper, a structure scheme of coaxial integrated macro-micro composite actuator is proposed. Based on the analysis method of "circuit", its macro magnetic field model is established and validated by electromagnetic field simulation. The results show that the simulation results agree with the calculation results of the established model, which shows the correctness of the established macro magnetic field model. It is reasonable and feasible

to combine the large stroke of voice coil motor with the high precision advantage of super magnetostrictive drive and put forward a scheme of coaxial integrated macro-micro composite actuator with large stroke and high precision.

Acknowledgements

This work is supported by Anhui Provincial Natural Science Foundation (No. 2008085QE214 and 1908085-ME159) and China Postdoctoral Science Foundation (No. 2019M652159) and Natural Science Research Projects of Colleges and Universities in Anhui Province (No. KJ2019A0111) and Youth Natural Science Foundation of Anhui University of Science and Technology (No. QN2018102 and QN2019117).

References

[1] N. A. Committee, Beijing: Electronic Industry Press (2018).
[2] M. E. Science, Beijing: Science Press, 10 (2010).
[3] C. Yu, C. Wang, T. Xie, L. Yang, and Z. Jiang, J. Mech. Eng. **55**, 136 (2019).
[4] C. Yu, C. Wang, H. Deng, T. He, and C. Zhong, J. Rare Earths **34**, 882 (2016).
[5] J. Yuan, G. S. Fox-Rabinovich, and S. C. Veldhuis, Wear. S 402 (2018).
[6] T. Weichelt, Y. Bourgin, and U. D. Zeitner, Opt. Express. **25**, 20983 (2017).
[7] K. Kawashima, Int. J. Urol. **25**, 103 (2018).
[8] H. J. Pahk, D. S. Lee, and J. H. Park, Int. J. Mach. Tool. Manu. **41**, 51 (2001).
[9] S. Lu, K. Yang, Y. Zhu, L. Wang, M. Zhang, and J. Yang, Acta Optic. Sin. **37**, 202 (2017).
[10] L. Wang, B. Su, and S. Dong, China Mech. Eng. **13**, 201 (2002).
[11] T. Zhang, S. Li, L. Li, Y. Liao, F. Cao, and S. Wen, J. Vib. Meas. Diag. **37**, 692 (2017).
[12] X. Bai, F. Cai, and P. Chen, Mech. Syst. Singal Pr. **117**, 157 (2019).
[13] P. Chen, X. Bai, L. Qian, and S. Choi, IEEE-ASME T. Mech. **23**, 1270 (2018).
[14] L. Zhang, Z. Long, L. Nian, and J. Fang, China Mech. Eng. **25**, 3088 (2014).
[15] C. Xu, J. Duan, H. Tang, S. Li, and J. Cen, Sou. Uni. (Sci. Tech.) **1**, 80 (2018).
[16] J. Zhang, Y. Liu, Y. Guo, J. Liu, and Y. Uchida, J. Mech. Eng. **47**, 187 (2011).
[17] W. Teng, H. Mu, and Y. Zhou, J. Mech. Eng. **50**, 165 (2014).